



ANM2017

## Photoreduction of nitrates from waste and drinking water

Elnaz Bahadori<sup>a</sup>, Matteo Compagnoni<sup>a</sup>, Antonio Tripodi<sup>a</sup>, Francesca Freyria<sup>b</sup>,  
Marco Armandi<sup>b</sup>, Barbara Bonelli<sup>b</sup>, Gianguido Ramis<sup>c</sup>, Ilenia Rossetti<sup>a,\*</sup>

<sup>a</sup> Chemical Plants and Industrial Chemistry Group, Dep. of Chemistry, Università degli Studi di Milano, CNR-ISTM and INSTM-Milano  
Università unit, Via C. Golgi 19, Milano, Italy

<sup>b</sup> Dept. of Applied Science and Technology, and INSTM-Unit Torino-Politecnico, Politecnico di Torino, C.so Duca degli Abruzzi 24, I-10129  
Torino, Italy

<sup>c</sup> Dip. di Ingegneria Civile, Chimica e Ambientale, Università degli Studi di Genova, P.le J.F. Kennedy 1, I-16129, Genova, Italy and INSTM  
Unit Genova

---

### Abstract

The photoreduction of nitrate ions was studied for the abatement of N-containing compounds from waste and drinking water. A new process was developed in semibatch mode, aiming at maximum selectivity towards N<sub>2</sub>. Different photocatalysts have been prepared with two different methods and their photocatalytic performance has been compared with commercial nanostructured TiO<sub>2</sub> (P25). TiO<sub>2</sub> has been prepared in nanosized form by using an innovative flame pyrolysis (FP) approach, and mesoporous TiO<sub>2</sub> was prepared by sol-gel method. Pd has been added to TiO<sub>2</sub> by post synthesis impregnation. The physical/chemical properties of the photocatalysts were studied by means of XRD, BET and UV-Vis spectroscopy.

The results show that the flame pyrolysis procedure is a viable technique for the preparation of nanosized TiO<sub>2</sub> for this application, leading to *ca.* double conversion with respect to P25. Furthermore, the addition of a small amount of Pd (0.1 mol %), likely enhanced the lifetime of the photoproducted charges by electron trapping and resulted in higher conversion and selectivity toward N<sub>2</sub>. The best performance was obtained with Pd doped on TiO<sub>2</sub> (FP), with 13% conversion and *ca.* 27% selectivity, only, toward ammonia formation.

© 2017 The Authors. Published by Elsevier Ltd. This is an open access article under the CC BY-NC-ND license (<http://creativecommons.org/licenses/by-nc-nd/4.0/>).

Selection and/or Peer-review under responsibility of ANM2017.

*Keywords:* Photoreduction nitrate; TiO<sub>2</sub>; Water depuration; Photocatalysis; Pd-doping

---

\* Corresponding author. Fax: +39-02-50314300.

E-mail address: [Ilenia.rossetti@unimi.it](mailto:Ilenia.rossetti@unimi.it)

## 1. Introduction

Nitrogen containing compounds, such as dyes, pesticides, drugs, etc. as well as inorganic ammonia (1), nitrites and nitrates (2), are harmful contaminants for drinking and waste waters (3). These compounds are particularly relevant in agriculturally intensive zones and in the case of some industrial processes involving e.g. nitrification reactions. Naturally, the nitrite ion is also usually formed by ammonia oxidation through nitrite bacteria (4). The development of effective methods for the abatement of these harmful pollutants from waste waters and from hydric resources is a challenging task. The reduction of  $\text{NO}_3^-$  and  $\text{NO}_2^-$  through catalytic, electrocatalytic and photocatalytic processes have been studied, however, the over-reduction to  $\text{NH}_3/\text{NH}_4^+$  and, thus, minor selectivity toward  $\text{N}_2$  still remains the main issue (5, 6) (Reactions 1-3).



Co-catalysts, such as Cu or Sn, Pd (7-9) usually improve the conversion by reducing the band gap and shifting light harvesting towards the visible part of the spectrum (10-12). Pd is particularly active (13, 14), since better charge-transfer between the metal and the semiconductor is expected, therefore, enhancing charge separation (15, 16).

Different production techniques can be used for  $\text{TiO}_2$ , e.g. leading to mesoporous  $\text{TiO}_2$  ( $\text{TiO}_2$ -meso) (17, 18) or flame spray pyrolysis ( $\text{TiO}_2$ -FP) to achieve dense nanoparticles of  $\text{TiO}_2$  (19, 20). Due to the abundance of oxygen and high temperature in the FSP reactor, the nanoparticles produced by FP are typically fully oxidized and highly crystalline. Likewise, in mesoporous  $\text{TiO}_2$  reducing the pore size to the meso range (2–50 nm) and increasing the surface area (21), enhance the photocatalytic properties (22). Furthermore, a proper arrangement can further assist the electron/energy transport within the mesoporous framework (23, 24).

The aim of this study is to compare  $\text{TiO}_2$ -based photocatalysts obtained by FP and sol-gel methods with P25. The effect of Pd-doping and the addition of acid formic as hole scavenger were also investigated.

## 2. Experimental

### 2.1. Materials preparation

Different  $\text{TiO}_2$  samples were prepared in dense nanostructured form by flame pyrolysis (19, 20) and in mesoporous form by sol-gel synthesis (17, 18). They were compared with a commercial P25 sample supplied by Evonik (code  $\text{TiO}_2$ - P25).

The FP-prepared sample (code  $\text{TiO}_2$ -FP) was prepared using a home-developed apparatus, constituted by a burner where a solution of the oxide precursor in organic solvent is fed through a syringe pump at constant feeding rate of 2.5 ml/min. The burner is co-fed with 5 L/min of oxygen and the flame is ignited and sustained by a ring of flamelets (0.5 L/min  $\text{CH}_4$  + 1 L/min of  $\text{O}_2$ ). The precursors solution was prepared by dissolving Titanium Isopropoxide (Sigma Aldrich, pur. 97%) as  $\text{TiO}_2$  precursor in o-xylene and Propionic acid (Sigma Aldrich, pur. 97%) with a 0.4 M concentration. The pressure drop at the burner nozzle was 1.5 bar.

The mesoporous  $\text{TiO}_2$  sample (code  $\text{TiO}_2$ -meso) was prepared by soft-template synthesis. ACS (American Chemical Society) grade chemicals from Sigma-Aldrich (Milan, Italy) were used as reactants. A first solution (A) was obtained by adding dropwise 5.0 g  $\text{Ti}(\text{O}i\text{Bu})_4$  (titanium tert-butoxide) to 30.0 mL of acetic acid (20%, v/v) and the mixture was then vigorously stirred for about 4 h. Solution B was obtained by mixing 3.0 g Pluronic P123 and ca. 20.0 mL ethanol. Solution B was then added dropwise to solution A: the resulting mixture was sealed, stirred for 24 h at r.t. and transferred into a Teflon autoclave for hydrothermal treatment at 95 °C for 48 h. The solid was centrifuged, dried at 80 °C and calcined in air at 450 °C for 4 h. Pd was added by impregnation from an aqueous solution of  $\text{Pd}(\text{NO}_3)_2$  in 0.1 mol % loading for each sample. Pd reduction was accomplished by treatment in  $\text{H}_2$  flow at 300 °C for 3h. The reduction temperature was preliminarily checked by TPR.

## 2.2. Materials characterization

X-ray diffraction (XRD) experiments were performed on a Rigaku D III-MAX horizontal-scan powder diffractometer with Cu-K $\alpha$  radiation, equipped with a graphite monochromator on the diffracted beam.

N<sub>2</sub> adsorption and desorption isotherms were collected with a Micromeritics ASAP2020 apparatus.

Diffuse Reflectance (DR) UV-Vis spectra of samples were measured on a Cary 5000 UV-Vis-NIR spectrophotometer (Varian instruments) in the range of 200–800 nm.

TPR analysis was carried out on a bench scale apparatus by flowing 40 ml/min of a 10 vol% H<sub>2</sub>/N<sub>2</sub> mixture, while heating the sample by 10 °C/min up to 700°C. The gas outflowing the quartz reactor was analysed by with a TCD detector after entrapping the possibly formed water.

## 2.3. Photoreactor and testing conditions

A newly designed photoreactor was employed for nitrate reduction testing. It is constituted by a pyrex cylinder with a cooling jacket, where water is continuously flowing. The reactor is externally irradiated with a UV lamp (Jelosil, 250 W, maximum emission at 365 nm, mean irradiance = 65 W/m<sup>2</sup>) placed on the top, through a quartz window. This design, though less efficient than annular reactors with immersion lamps, allows easier modelling and scale up. Above all, in view of transition to solar energy it allows easier light harvesting.

250 ml of a 0.006 M NaNO<sub>3</sub> solution are loaded in the reactor, 250 mg of catalyst are suspended by magnetic agitation and the system is outgassed for 100 min by flowing He, which is also continuously fed during the whole activity test (semibatch mode). Then the lamp is switched on and samplings of the solution and of the gas phase are carried out periodically for 5 h.

Nitrite and nitrate ions are quantified by means of an ion chromatograph (Metrohm 883 Basic IC Plus), while the possibly formed ammonia is quantified by UV-Vis spectroscopy (Perkin Elmer Lambda 35) using the indophenol standard method. N<sub>2</sub> can be quantified in line by sampling the continuous He flow in a gaschromatograph (HP 5890), but due to the semicontinuous reaction mode it never accumulates sufficiently for detection.

The best performing catalyst was also tested with the addition of variable amounts of formic acid, selected as hole scavenger.

## 3. Results and discussion

### 3.1. Materials characterisation

The XRD pattern of TiO<sub>2</sub> sample obtained by flame pyrolysis shows a mixture of the crystalline phases of anatase and rutile (Figure 1). All the reflections were identified by comparison with the standard JCPDS spectrum of rutile (88-1175) and anatase (84-1286) (25). Both Pd doped and bare TiO<sub>2</sub> samples have the same XRD pattern, therefore, Pd loading did not have a significant influence on the crystal structure of TiO<sub>2</sub>. Furthermore, there were no reflections related to Pd in the patterns, due to very low loading and high dispersion of the metal.

For the mesoporous TiO<sub>2</sub> sample obtained with the sol-gel method, the XRD pattern shows the sole presence of the anatase phase, without any reflection corresponding to the other TiO<sub>2</sub> polymorphs.

The phase composition of each sample, as determined by XRD data, is reported in Table 1. According to the literature (26) by considering the intensity ratio between the most intense reflections of anatase at (101) and rutile at (110) plane, the percentage of both phases can be calculated as follows (Table 1):

$$\text{Anatase } (X_A) = \frac{1}{1 + 1.265 \frac{I_R}{I_A}}$$

$$\text{Rutile } (X_R) = \frac{1}{1 + 0.8 \frac{I_A}{I_R}}$$

The average particle size was also estimated from peak width at half maximum by using the Scherrer's equation (Table 1):

$$D_{hkl} = \frac{0.9\lambda}{\beta \cos \theta}$$

where  $D_{hkl}$  is the average crystallite diameter,  $\lambda$  is wavelength of X-rays = 0.1541874 nm,  $\beta$  full width at half maximum in radians and 0.9 is a correction for instrumental line broadening.

The average crystallite sizes of TiO<sub>2</sub> nanoparticles were determined from the broadening of the (101) peak at ( $2\theta = 25.3^\circ$ ) (Table 1) (27). The mesoporous titania sample revealed much smaller crystallites with respect to the FP prepared sample due to the lower temperature achieved during the synthesis. By contrast, the P25 and FP samples has comparable crystal size and approximately similar phase composition.

To determine the BET SSA (Brunauer-Emmett-Teller Specific Surface Area) and porous volume, N<sub>2</sub> adsorption/desorption isotherms were collected at -196 °C on every sample, previously outgassed at 150 °C for 4h. Microporous volume was calculated according to the *t*-plot method. The results are reported in Table 2.

Table 1. Crystal phases and crystallite size quantification from XRD data through the Scherrer equation.

Samples	Anatase	Rutile	2 $\theta$	FWHM (°)*	FWHM (rad)	Crystal Size (nm)
Pd-TiO <sub>2</sub> -meso	100	0	25.2	0.917	0.0160	9
Pd-TiO <sub>2</sub> -P25	57.8	42	25.2	0.465	0.0081	17
Pd-TiO <sub>2</sub> -FP	53.2	46.8	25.3	0.436	0.0076	18
TiO <sub>2</sub> -FP	68.6	31.3	25.3	0.404	0.0070	20

\*FWHM=Full Width at Half Maximum

Table 2. Textural properties as determined from N<sub>2</sub> sorption isotherms at -196 °C.

Sample	BET Surface area (m <sup>2</sup> g <sup>-1</sup> )	BJH Adsorption cumulative surface area (m <sup>2</sup> g <sup>-1</sup> )	t-Plot Micropore Area (m <sup>2</sup> g <sup>-1</sup> )	Total pore volume (cm <sup>3</sup> g <sup>-1</sup> )	t-Plot micropore volume (cm <sup>3</sup> g <sup>-1</sup> )	Adsorption average width (nm)	BJH Adsorption average pore width (nm)
TiO <sub>2</sub> -P25	45	38	23	0.12	0.01	10	22
TiO <sub>2</sub> -meso	128	159	-	0.28	0.00	9	7
Pd-TiO <sub>2</sub> -meso	128	158	-	0.27	0.00	8	7
TiO <sub>2</sub> -FP	67	44	41	0.14	0.02	8	20
Pd-TiO <sub>2</sub> -FP	57	59	3	0.21	0.00	14	14

The TiO<sub>2</sub> obtained by flame pyrolysis and Pd doped one, both show a type II isotherm with H1 hysteresis loop, representing the unrestricted monolayer-multilayer adsorption through the agglomerates or spherical particles arranged uniformly with high pore size uniformity and facile pore connectivity (28). On the contrary, the mesoporous samples (TiO<sub>2</sub> and Pd doped TiO<sub>2</sub>) show type IV isotherms with H2 characteristic hysteresis loop extending from the medium to high pressure zone ( $0.6 < P/P_0 < 0.9$ ). This is attributed to a non-homogeneous mesoporous network and to the existence of a macropore structure with channel-like pores and network connectivity (28).

The mesoporous TiO<sub>2</sub> samples showed the highest BET surface area with respect to the FP and commercial P25 samples (Table 2). The surface area was even higher than the ones reported in the literature (17, 29), which can be advantageous for the adsorption of a larger amount of reactant and, therefore, for conversion improvement.

The porosity of the samples were also markedly different. The mesoporous sample had a negligible contribution of micropores, whereas some microporosity was ascribed to both the FP (higher) and P25 samples (lower). The primary particles were essentially dense in both cases, but a fine network of micropores derives from their coalescence. However, some microporosity is lost upon Pd addition to the FP-prepared TiO<sub>2</sub>.

Table 3. Band gap calculation from DR UV-Vis data elaborated according to Tauc plots.

Sample	Band Gap energy (eV)
P <sub>25</sub>	3.36
Pd-TiO <sub>2</sub> -P <sub>25</sub>	3.16
TiO <sub>2</sub> -FP	3.36
Pd-TiO <sub>2</sub> -FP	3.13
TiO <sub>2</sub> -meso	3.22
Pd-TiO <sub>2</sub> -meso	3.03

Figures 2 and 3 show the UV-Vis spectra of different types of TiO<sub>2</sub> (P25, FP and mesoporous) and the relative Pd-doped samples.

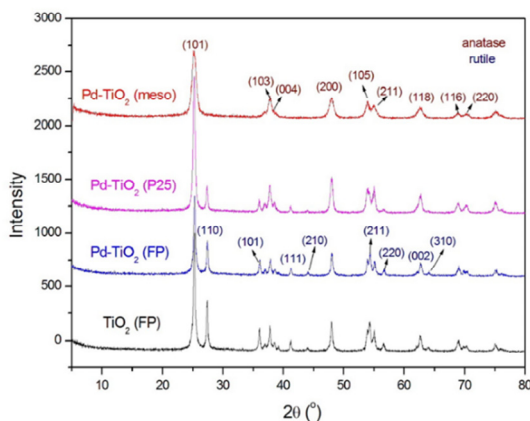


Fig. 1. XRD patterns of TiO<sub>2</sub>-FP and Pd-doping (0.1 mol %) on different TiO<sub>2</sub> samples.

According to UV absorption spectra, all the samples show an intense absorption in the spectral range between 240–380 nm, due to electron transfer from the 2p valence band orbital of O to the 3d conduction band orbital of Ti (7, 30). The spectra of un-doped TiO<sub>2</sub> samples show the cut-off at shorter wavelengths, with respect to the doped samples. The main reason for the observed bathochromic shift in transition and the visible light absorption is due to changing of the energy levels of the semiconductor band gap through a charge transfer between the metal conduction band and the valence band or the d–d transition in the crystal field (27, 31).

The optical band gap energy  $E_g$  was determined according to the Tauc equation (32, 33). The direct band gap energy can be estimated from a plot of  $(\alpha h\nu)^2$  versus the photon energy ( $h\nu$ ). The energy band gap is reported in Table 3 and it was determined as follows:

$$\begin{aligned} \alpha h\nu &= A(h\nu - E_g)^n \\ (\alpha h\nu)^2 &= A(h\nu - E_g) \end{aligned}$$

where  $h\nu$  = photon energy,  $\alpha$  = absorption coefficient,  $E_g$  = energy band gap,  $A$  = constant and  $n = 1/2$  for the allowed direct band gap. The exponent  $n$  depends on the type of transition and it may assume the values  $1/2$ ,  $2$ ,  $3/2$  and  $3$  corresponding to the allowed direct, allowed indirect, forbidden direct, and forbidden indirect transitions, respectively (27, 34).

According to the  $E_g$  calculations (Table 3) by doping the  $\text{TiO}_2$  samples with Pd, the absorption has been extended to longer wavelengths and the band gap energy reduced (7, 35).

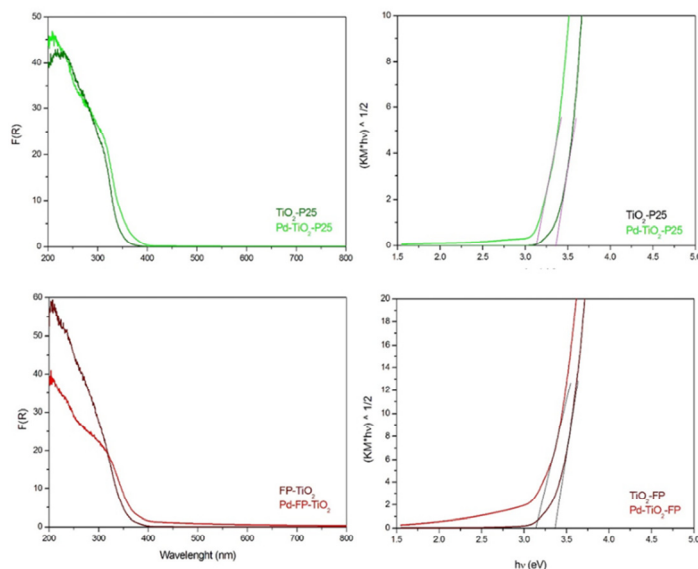


Fig. 2. Top: DR UV-Vis spectra (left) and corresponding Tauc plots (right) of  $\text{TiO}_2\text{-P25}$  and  $\text{Pd-TiO}_2\text{-P25}$ . Bottom: DR UV-Vis spectra (left) and corresponding Tauc plots (right) of  $\text{TiO}_2$  obtained by Flame Pyrolysis and doped with Pd (0.1 mol %).

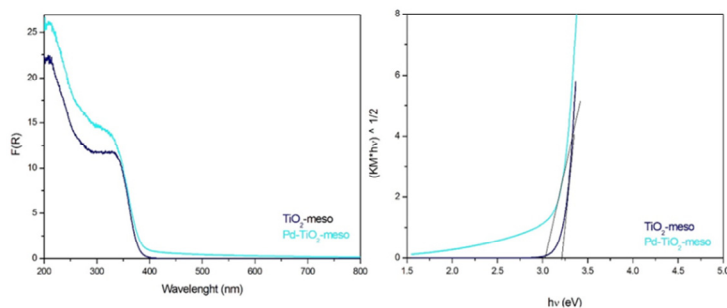


Fig. 3: DR UV-Vis spectra (left) and corresponding Tauc plots (right) of mesoporous  $\text{TiO}_2$  obtained by synthesis and doped with Pd (0.1 mol%)

By comparing the undoped samples, a peculiar behavior was observed. On one hand the P25 and FP  $\text{TiO}_2$  samples were characterized by the same band gap. This is reasonable since they have a very similar phase composition (30–40% rutile and 60–70% anatase) and rather similar crystal size. By contrast, the mesoporous  $\text{TiO}_2$  sample unexpectedly showed the lowest band gap, although it is constituted by pure anatase (which has higher band gap than rutile) and the smallest crystal size. It is indeed known that the band gap should increase with decreasing crystal size (36, 37). This behavior can be interpreted on the basis of the absorption pattern reported in Fig 3, which evidences two neat absorption features, one of them sharply shifted towards the visible absorption edge.

Furthermore, the mesoporous structure of titania may assist the electron/hole transportation within the framework by formation a short distance for moving the photogenerated charges carries the catalytic sites (7, 38).

### 3.2. Photoreduction of nitrate ions

#### 3.2.1 – Effect of catalyst formulation and preparation procedure

The photoreduction of nitrates has been tested with the bare  $\text{TiO}_2$  photocatalysts described above. Very low conversion of nitrates was observed with 100% selectivity toward the undesired ammonia, which is produced through the undesired consecutive reactions (Reactions 1-3). The  $\text{TiO}_2$ -meso, however, shows the higher conversion (4.4 %) with respect to the other photocatalysts ( $\text{TiO}_2$ -FP ca. 1/ nitrate conversion after 5 h, while P25 led to negligible conversion). The overall activity scale strictly followed the surface area trend. Apparently, the mixed anatase + rutile structures (samples P25 and FP) were in general less performing than pure anatase, but sample P25 was characterized by higher anatase content, while it was substantially not active. Thus the effect of surface area seems prevailing over the structural one.

As above discussed, Pd was added in a small quantity (0.1 mol %) by post synthesis impregnation on all the titania samples. The activity and selectivity of the Pd-doped  $\text{TiO}_2$  samples (meso and FP, as they led to some conversion when unpromoted) are reported in Figure 4. Considerably higher conversion of nitrates was achieved for every sample. A much higher improvement of conversion was observed for the Pd-FP sample, whereas for the mesoporous catalyst the conversion was ca. doubled upon Pd addition. However, the most relevant result was the improved selectivity to  $\text{N}_2$ , since selectivity toward ammonia, as a by-product, although still relevant, considerably decreased upon Pd promotion.

According to band gap calculations, Pd decreased the bandgap energy of the catalyst, which in turn increased the light harvesting efficiency and, thus, resulted in higher conversion for all photocatalysts. The best performance was obtained with Pd- $\text{TiO}_2$ -FP, with 13% conversion and ca. 27% selectivity toward ammonia.

Even though mesoporous  $\text{TiO}_2$  showed a pure anatase phase which has been reported to have a higher photocatalytic activity with respect to the rutile phase, the photocatalytic activity of  $\text{TiO}_2$  materials consisting in a mixture of anatase and rutile is known to be enhanced by better electrons and holes separation (39). Indeed, the synergism between the different crystalline phases, promotes the migration of photogenerated charges, thus helping their separation and improving their lifetime (40).

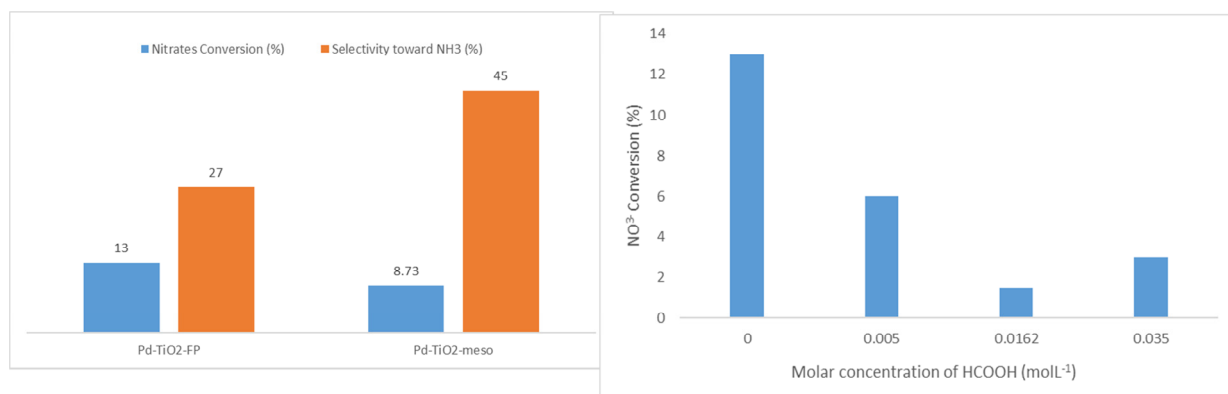


Figure 4: Left: Nitrates conversion and selectivity toward  $\text{NH}_3$  for the Pd doped  $\text{TiO}_2$  photocatalysts. Right: Nitrates conversion with Pd- $\text{TiO}_2$ -FP photocatalyst and different concentrations of acid formic.

### 3.2.2 – Effect of hole scavengers addition

The best catalyst in terms of higher conversion (*i.e.* Pd- TiO<sub>2</sub>-FP sample) was then used to investigate the effect of hole scavengers on the photocatalytic process. Hole scavengers are often added to improve the rate of photoreduction reactions. Indeed, the photopromoted electron is used for the reduction half reaction. In this case the interest is on the reduction of nitrates, while in the literature various examples are reported for the reduction of H<sup>+</sup> to H<sub>2</sub> or of CO<sub>2</sub> to regenerated fuels (41-44). Substantially, the addition of a hole or electron scavenger to the reaction system is used in combination with the deposition of metals on the TiO<sub>2</sub> surface to overcome the rapid charges recombination rate.

Formic acid has been added in three different concentrations into the reaction medium. The results have been reported in Figure 4.

Formic acid as hole scavenger has been studied to enhance the photocatalytic reduction of aqueous Pb(II) over Ag doped TiO<sub>2</sub> (45), as well as reduction of Se(VI) and Se(IV) to elemental Se onto TiO<sub>2</sub> surface (46). Formic acid has a fast mineralization rate, the ability to form reducing radicals quickly, which increases its efficiency in the photochemical reactions as a hole scavenger. However, for the present tests of nitrates photoreduction, adding formic acid as a hole scavenger resulted in lower conversion (Figure 4, right) and, most of all, in 100 % selectivity toward ammonia. The proposed catalyst is very active also for H<sub>2</sub> production and CO<sub>2</sub> photoreduction, which are both strongly enhanced by the presence of formic acid in the reaction medium (41), so that the photoreduction of nitrate has to compete with reactions which are strongly favored by HCOOH addition.

## 4. Conclusions

A photoreactor has been set up for studying the photoreduction of nitrates in semibatch mode. The specific configuration of designed photoreactor with the possibility to be further optimised in a terms of geometry and mixing, opens a possibility for scale up, easily implements immobilised photocatalysts and operation with the direct sunlight.

The bare TiO<sub>2</sub> photocatalysts, was much less active during the photoreduction of nitrate, requiring the addition of a small amount of Pd to achieve interesting conversion. The addition of the noble metal, besides improving conversion, also allowed to enhance the selectivity to N<sub>2</sub>, limiting the undesired formation of ammonia, the only observed product with the undoped titania catalysts.

Comparing the photoreduction conversion and selectivity, the flame pyrolysis procedure demonstrated a viable technique for the preparation of metal-doped semiconductors in nanosized form, to be used for the photocatalytic abatement of inorganic N-containing pollutants in waste or drinking waters.

On the other hand, the addition of HCOOH as a hole scavenger negatively affected the nitrate conversion and led to unacceptably high selectivity toward ammonia. This was explained in terms of competition with rivalling reactions that are more promptly favoured by formic acid addition.

## Acknowledgements

The authors are grateful to Fondazione Cariplo (Italy) for financial support through the grant 2015-0186 “DeN – Innovative technologies for the abatement of N-containing pollutants in water”.

I. Rossetti and E. Bahadori are grateful to Fondazione Cariplo and Regione Lombardia for financial support through the grant 2016-0858 – “Up-Unconventional Photoreactors”.

## References

1. Lee J, Park H, Choi W, Selective Photocatalytic Oxidation of NH<sub>3</sub> to N<sub>2</sub> on Platinized TiO<sub>2</sub> in Water, *Environmental Science & Technology*. 36 (2002) 5462-5468.
2. Nolan BT, Puckett LJ, Ma L, Green CT, Bayless ER, Malone RW, Predicting Unsaturated Zone Nitrogen Mass Balances in Agricultural Settings of the United States All rights reserved, *Journal of Environmental Quality*. 39 (2010) 1051-1065.

3. Burow KR, Nolan BT, Rupert MG, Dubrovsky NM. Nitrate in Groundwater of the United States, 1991–2003, *Environmental Science & Technology*. 44 (2010) 4988–4997.
4. Tiso M, Schechter AN, Nitrate Reduction to Nitrite, Nitric Oxide and Ammonia by Gut Bacteria under Physiological Conditions, *PLoS One*. 10 (2015) e0119712.
5. Kim M-S, Chung S-H, Yoo C-J, Lee MS, Cho I-H, Lee D-W, et al, Catalytic reduction of nitrate in water over Pd–Cu/TiO<sub>2</sub> catalyst: Effect of the strong metal-support interaction (SMSI) on the catalytic activity, *Appl. Catal., B: Environ.* 142 (2013) 354–361.
6. Shand M, Anderson JA, Aqueous phase photocatalytic nitrate destruction using titania based materials: routes to enhanced performance and prospects for visible light activation, *Cat Sci & Technol*. 3 (2013) 879–899.
7. Seifvand N, Kowsari E, Synthesis of Mesoporous Pd-Doped TiO<sub>2</sub> Templated by a Magnetic Recyclable Ionic Liquid for Efficient Photocatalytic Air Treatment, *Industrial & Engineering Chemistry Research*. 55 (2016) 10533–10543.
8. Karvinen SM, The Effects of Trace Element Doping on the Optical Properties and Photocatalytic Activity of Nanostructured Titanium Dioxide, *Industrial & Engineering Chemistry Research*. 42 (2003) 1035–1043.
9. Aristizábal A, Contreras S, Barrabés N, Llorca J, Tichit D, Medina F, Catalytic reduction of nitrates in water on Pt promoted Cu hydroxalate-derived catalysts: Effect of the Pt–Cu alloy formation, *Appl. Catal., B: Environ.* 110 (2011) 58–70.
10. Chen Y-H, Franzreb M, Lin R-H, Chen L-L, Chang C-Y, Yu Y-H, et al, Platinum-Doped TiO<sub>2</sub>/Magnetic Poly(methyl methacrylate) Microspheres as a Novel Photocatalyst, *Industrial & Engineering Chemistry Research*. 48 (2009) 7616–7623.
11. Biyoghe Bi Ndong L, Ibondou MP, Gu X, Lu S, Qiu Z, Sui Q, et al, Enhanced Photocatalytic Activity of TiO<sub>2</sub> Nanosheets by Doping with Cu for Chlorinated Solvent Pollutants Degradation, *Industrial & Engineering Chemistry Research*. 53 (2014) 1368–1376.
12. Kumaresan L, Mahalakshmi M, Palanichamy M, Murugesan V, Synthesis, Characterization, and Photocatalytic Activity of Sr<sup>2+</sup> Doped TiO<sub>2</sub> Nanoplates, *Industrial & Engineering Chemistry Research*. 49 (2010) 1480–1485.
13. Yashima M, Falk LKL, Palmqvist AEC, Holmberg K, Structure and catalytic properties of nanosized alumina supported platinum and palladium particles synthesized by reaction in microemulsion, *Journal of Colloid and Interface Science*. 268 (2003) 348–356.
14. Liu X, Wang R, Song L, He H, Zhang G, Zi X, et al, The oxidation of carbon monoxide over the palladium nanocube catalysts: Effect of the basic-property of the support, *Catalysis Communications*. 46 (2014) 213–218.
15. Ma D, Yan Y, Ji H, Chen C, Zhao J, Photocatalytic activation of pyridine for addition reactions: an unconventional reaction feature between a photo-induced hole and electron on TiO<sub>2</sub>, *Chemical Communications*. 51 (2015) 17451–1754.
16. González CA, Bartoszek M, Martin A, Correa CMD, Hydrodechlorination of Light Organochlorinated Compounds and Their Mixtures over Pd/TiO<sub>2</sub>-Washcoated Minimonoliths, *Industrial & Engineering Chemistry Research*. 48 (2009) 2826–2835.
17. Muniz EC, Góes MS, Silva JJ, Varela JA, Joanni E, Parra R, et al, Synthesis and characterization of mesoporous TiO<sub>2</sub> nanostructured films prepared by a modified sol–gel method for application in dye solar cells, *Ceramics International*. 37 (2011) 1017–1024.
18. Freyria FS, Compagnoni M, Ditaranto N, Rossetti I, Piumetti M, Ramis G, et al, Pure and Fe-Doped Mesoporous Titania Catalyse the Oxidation of Acid Orange 7 by H<sub>2</sub>O<sub>2</sub> under Different Illumination Conditions: Fe Doping Improves Photocatalytic Activity under Simulated Solar Light, *Catalysts*. 7 (2017).
19. Compagnoni M, Lasso F J, Di Michele A, Rossetti I, Flame-pyrolysis-prepared catalysts for the steam reforming of ethanol, *Catalysis Science & Technology*. 6 (2016) 6247–6256.
20. Chiarello GL, Rossetti I, Forni L, Flame-spray pyrolysis preparation of perovskites for methane catalytic combustion, *Journal of Catalysis*. 236 (2005) 251–261.
21. Tobaldi DM, Pullar RC, Duraes L, Matias T, Seabra MP, Labrincha JA, Truncated tetragonal bipyramidal anatase nanocrystals formed without use of capping agents from the supercritical drying of a TiO<sub>2</sub> sol, *CrystEngComm*. 18 (2016) 164–176.
22. Tian G, Fu H, Jing L, Xin B, Pan K, Preparation and Characterization of Stable Biphasic TiO<sub>2</sub> Photocatalyst with High Crystallinity, Large Surface Area, and Enhanced Photoactivity, *J. Phys Chem C*. 112 (2008) 3083–3089.
23. Bu J, Fang J, Leow WR, Zheng K, Chen X, Single-crystalline rutile TiO<sub>2</sub> nano-flower hierarchical structures for enhanced photocatalytic selective oxidation from amine to imine, *RSC Advances*. 5 (2015) 103895–103900.

24. Liao Y-T, Huang C-W, Liao C-H, Wu JCS, Wu KCW, Synthesis of mesoporous titania thin films (MTTFs) with two different structures as photocatalysts for generating hydrogen from water splitting, *Applied Energy*. 100 (2012) 75-80.
25. Thamaphat K, Limsuwan P, Ngotawornchai B. Phase Characterization of TiO<sub>2</sub> Powder by XRD and TEM, *Kasetsart J (Nat Sci)*. 42 (2008) 4.
26. Spurr RA, Myers H, Quantitative Analysis of Anatase-Rutile Mixtures with an X-Ray Diffractometer, *Analytical Chemistry*. 29 (1957) 760-762.
27. Chauhan R, Kumar A, Chaudhary RP, Structural and optical characterization of Ag-doped TiO<sub>2</sub> nanoparticles prepared by a sol-gel method, *Research on Chemical Intermediates*. 38 (2012) 1443-1453.
28. Thommes M, Kaneko K, Neimark Alexander V, Olivier James P, Rodriguez-Reinoso F, Rouquerol J, et al, Physisorption of gases, with special reference to the evaluation of surface area and pore size distribution (IUPAC Technical Report), *Pure Appl. Chem*. 87 (2015) 1051–1069.
29. Yu J, Yu JC, Ho W, Jiang Z, Effects of calcination temperature on the photocatalytic activity and photo-induced super-hydrophilicity of mesoporous TiO<sub>2</sub> thin films, *New Journal of Chemistry*. 26 (2002) 607-613.
30. Tan ST, Chen BJ, Sun XW, Fan WJ, Kwok HS, Zhang XH, et al, Blueshift of optical band gap in ZnO thin films grown by metal-organic chemical-vapor deposition, *J. Appl. Phys*. 98 (2005) 013505.
31. Hoffmann MR, Martin ST, Choi W, Bahnemann DW, Environmental Applications of Semiconductor Photocatalysis, *Chemical Reviews*. 95 (1995) 69-96.
32. Li P, Hu H, Xu J, Jing H, Peng H, Lu J, et al, New insights into the photo-enhanced electrocatalytic reduction of carbon dioxide on MoS<sub>2</sub>-rods/TiO<sub>2</sub> NTs with unmatched energy band, *Appl. Catal., B: Environ*. 147 (2014) 912-919.
33. Harikishore M, Sandhyarani M, Venkateswarlu K, Nellaippan TA, Rameshbabu N, Effect of Ag Doping on Antibacterial and Photocatalytic Activity of Nanocrystalline TiO<sub>2</sub>, *Procedia Materials Science*. 6 (2014) 557-566.
34. Pankove JI, I. J. Optical processes in semiconductors. N.J: Prentice-Hall, Englewood Cliffs; 1971.
35. Mogal SI, Gandhi VG, Mishra M, Tripathi S, Shripathi T, Joshi PA, et al, Single-Step Synthesis of Silver-Doped Titanium Dioxide: Influence of Silver on Structural, Textural, and Photocatalytic Properties, *Industrial & Engineering Chemistry Research*. 53 (2014) 5749-5758.
36. Rino J-P, Studart N, Structural correlations in titanium dioxide, *Physical Review B*. 59 (1999) 6643-6649.
37. Lin H, Huang CP, Li W, Ni C, Shah SI, Tseng Y-H, Size dependency of nanocrystalline TiO<sub>2</sub> on its optical property and photocatalytic reactivity exemplified by 2-chlorophenol, *Appl. Catal., B: Environ*. 68 (2006) 1-11.
38. Islam S, Nagpure S, Kim D, Rankin S, Synthesis and Catalytic Applications of Non-Metal Doped Mesoporous Titania, *Inorganics*. 5 (2017) 15.
39. Giannouri M, Kalampaliki T, Todorova N, Giannakopoulou T, Boukos N, Petrakis D, et al, One-Step Synthesis of TiO<sub>2</sub>/Perlite Composites by Flame Spray Pyrolysis and Their Photocatalytic Behavior, *International Journal of Photoenergy*. 2013.
40. Kho YK, Iwase A, Teoh WY, Madler L, Kudo A, Amal R, Photocatalytic H<sub>2</sub> Evolution over TiO<sub>2</sub> Nanoparticles, The Synergistic Effect of Anatase and Rutile. *J. Phys. Chem. C*. 114 (2010) 2821-2829.
41. Galli F, Compagnoni M, Vitali D, Pirola C, Bianchi CL, Villa A, et al. CO<sub>2</sub> photoreduction at high pressure to both gas and liquid products over titanium dioxide. *Appl. Catal., B: Environ*. 200 (2017) 386-391.
42. Rossetti I, Villa A, Pirola C, Prati L, Ramis G, A novel high-pressure photoreactor for CO<sub>2</sub> photoconversion to fuels, *RSC Advances*. 4 (2014) 28883-28885.
43. Rossetti I, Villa A, Compagnoni M, Prati L, Ramis G, Pirola C, et al, CO<sub>2</sub> photoconversion to fuels under high pressure: effect of TiO<sub>2</sub> phase and of unconventional reaction conditions, *Catalysis Science & Technology*. 5 (2015) 4481-4487.
44. Rossetti I, Hydrogen Production by Photoreforming of Renewable Substrates, *ISRN Chemical Engineering*. 2012 (2012) 21.
45. Li L, Jiang F, Liu J, Wan H, Wan Y, Zheng S, Enhanced photocatalytic reduction of aqueous Pb(II) over Ag loaded TiO<sub>2</sub> with formic acid as hole scavenger, *J. Environmental Science & Health, Part A*. 47 (2012) 327-336.
46. Tan T, Beydoun D, Amal R, Effects of organic hole scavengers on the photocatalytic reduction of selenium anions, *Journal of Photochemistry and Photobiology A: Chemistry*. 159 (2003) 273-280.